Detection of Soft Atherosclerotic Plaques in Cardiac Computed Tomography Angiography

Muhammad Moazzam Jawaid
Department of Elec. & Electronics Engg.
City University London, EC1V0HB

Sajjad Ali Memon, Imran Ali Qureshi, Nasrullah Pirzada
Department of Telecommunication Engineering
Mehran University of Engineering & Technology, Jamshoro 76062

Abstract—**Computed tomography angiography (CTA) has turned non-invasive diagnosis of cardiovascular anomalies into a reality as state-of-the-art imaging equipment is capable of recording sub-millimeter details. Based on high intensity, the calcified plaques are easily identified in cardiac CTA; however, low density based non-calcified plaque detection has been a challenging problem in recent years. We propose an efficient method in this work for automated detection of the non-calcified plaques using discrete radial profiles. The plaque detection is accomplished using support vector machine to differentiate abnormal coronary segments. We investigated a total of 32 CTA volumes and the detection mean accuracy of 84.6% was achieved, which is in-line with the reported literature.**

Keywords—Coronary tree segmentation; support vector machines; non-calcified plaque detection; mean radial profiles; Rotterdam CTA dataset

I. Introduction

Coronary heart disease (CHD) refers to the deposition of materials (also termed as coronary plaques) inside coronary arteries. The growth of plaque results in a reduced blood flow towards heart muscles. Consequently, the heart muscles become oxygen starved resulting in fatal cardiac consequences including angina, heart failure and arrhythmias. In context of the flow of this paper, we present relevant literature in Section I-B, which is followed by the clinical data description. In the subsequent section, the proposed model is explained, followed with results of Section III. The last section presents some limitations and the future extension for this work.

A. Clinical Motivation

According to the fact sheet of the World Health Organization [1], CHD was the leading cause of death globally in 2013, with 8.14 million deaths (16.8%) compared to 5.74 million deaths (12%) in 1990. Moreover, the recent statistics of the National Health Services, United Kingdom [2] reveals that over 2.3 million people in the United Kingdom suffer from CHD where the annual death toll is approximately 73,000 (an average of one death every seven minutes). The huge levels of growing morbidity and mortality have led to a increased interest abnormality detection methods. From a clinical point of view, the detection and quantification of arterial plaque can help physicians avoid or at least delay the worst cardiac events by addressing behavioural risk factors [3]. State of the art developments [4] in non-invasive imaging technology have revolutionized the clinical diagnosis methods in recent years. For instance, sub-millimeter based acquisition of the internal organs has made CTA a feasible alternative to cardiac cauterization for detecting coronary obstruction [5]; however, the composition of the coronary plaques pose a difficult challenge in the effective diagnosis. High intensity calcified plaques can be detected easily in CTA imagery [6]–[9]; however, the detection of the non-calcified plaques has been a challenging problem in clinical practice due to close proximity with blood voxels.

Clinically, the non-calcified plaques have been established as the most important indicator of acute coronary syndromes due to their fragile nature [10]. Moreover, unexpected rupture has made soft plaques much threatening, i.e. for many individuals, sudden death becomes the first sign of soft plaque in contrast to the calcified plaques which often lead to disease symptoms at early stages. In addition, the positive remodeling associated with soft plaques further amplifies the detection challenge as the radial stenosis detection based methods often miss the non-calcified plaques [6]–[9], [11]. Consequently, the intense focus of the current research is an early detection of soft plaques to predict and avoid worst cardiac events [12].

B. Related Work

Based on the fact that soft plaque detection is a complex phenomena, there exists a little literature [13]–[17] addressing automatic detection of soft plaques in CTA imagery. Out of the reported work, the majority of the research have been clinical pilot studies or generic anomaly detection techniques. One framework in this context was proposed by Clouse *et al.* [13]; however the main focus was the quantification of manually identified soft plaques. Accordingly, a total of 49 coronary segments (41 normal, 8 abnormal) were chosen for investigation from a dataset of 40 CTA volumes, to validate the proposed quantification method. For precise quantification of soft plaques, the authors established correspondence between two normal cross sections at the terminal sites of the plaque region to approximate the outer boundary of the vessel. In the subsequent step, all voxels having intensity equal of the lumen were subtracted and those left over were identified as soft plaque. Accordingly, the research illustrated that the soft plaques can be quantified in CTA; however, the results were based on certain manual inputs i.e. a pre-selective set of the segments was used in investigation with a manual selection of plaque terminal points. An extension of this work further validated the quantification correlation among two imaging modalities (i.e. CTA and intravenous ultrasound (IVUS) plaque quantifications [18]. Similar to the base study, the selection of the coronary segment was made in a pre-processing stage for

optimal results. Accordingly, 20 soft plaque effected segments were chosen from a set of 12 CTAs. Despite of the successful correlation , this method does not fulfil the automated spirit as it was based on manual selection of the plaque positions.

Machine learning based soft plaque detection was first reported by Wei *et al.* [14], in which authors employed a linear discriminant analysis (LDA) to minimize the false positives for a set of 120 pre-selected plaque candidates. According, the efficiency of the LDA classifier was based on NCP candidate selection criteria, and the machine learning was used to maximize the performance by suppressing false candidates. Starting with a manually corrected coronary centreline, the vessel radius along the length of the centreline was obtained in the first stage. In a subsequent stage, the obtained radius was used to identify seed points for 2 mm long plaque candidate regions. From a set of 83 CTA volumes, 120 plaque candidate regions were used in detection process, for which the reported sensitivity was 92.5%. Another use of learning method was reported by Tessman [17], in which coronary stenosis effected cross-sections were detected. In the first step, the pre-extracted coronary centreline was used to map the vessel segment with a series of multi-scale overlapping cylinders to identify the sampling points inside the segment. Subsequently, image based features like intensity, gradient and the first-second order derivatives were extracted at the sampled points to identify high intensity calcifications. Moreover, global features including image mean, entropy and variance were used in combination with Haar-like features to detect the low intensity soft plaques. According to the reported results, the plaque detection accuracies were 94% and 79%, respectively for two classes of plaques i.e. calcified and non-calcified. It should be noted that the low accuracy for non-calcified plaques illustrate that soft plaque detection demands a more sophisticated system i.e. beyond stenosis based computations to efficiently address vessel remodelling.

An important method focusing on cross-section based vascular abnormality detection was proposed by Zuluaga *et al.* [19]. Based on the "density level detection" technique of Steinwart [20], authors employed an unsupervised learning approach in this work for detecting abnormal cross-section. In this method, the vascular cross-sectional images were discretely sampled around centreline to derive the feature set for suppressing outliers Subsequently, they used an SVM model trained on normal cross sections to label the outliers (i.e. the cross sections which violate the intensity pattern of normal class) as abnormal. According to the reported results, a good detection rate of 79.62%, was reported for 9 clinical CTA datasets; however, the selection of anomaly concentration parameter ρ plays an important role in overall results. In addition, a large number of normal cross-sections having similar intensity pattern are required for good training of SVM due to one-class nature of supervisor.

Similarly Renard and Yang [15], Lankton *et al.* [16] and Li *et al.* [21] proposed different approaches for the plaque detection in CTA; however, these method were validated for small datasets and require certain manual inputs from the user, which preclude the automated solutions. Likewise, a number of plaque quantification algorithms [22]–[25] have been proposed in recent years with a motive of correlating CTA with intra-vascular ultrasound (IVUS) measurements; however,

these methods again employ manual input in terms of the plaque position and length in respective coronary vasculature.
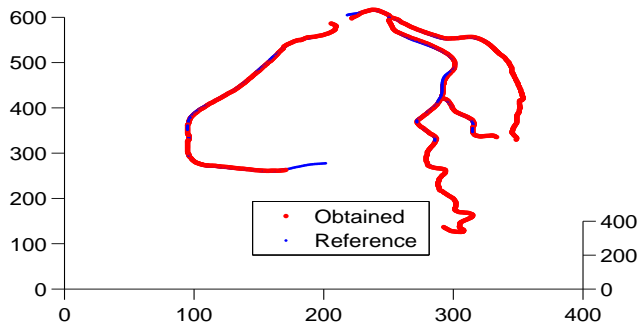
In contrast to manual input based quantification, we addressed the problem of automated detection of plaque in this work. Accordingly, our contribution is an efficient method for the detection of the non-calcified plaque in coronary vasculature. We employed a machine learning technique (SVM) for identifying non-calcified plaque affected coronary segments. It should be noted that the proposed method differs from LDA based Wei *et al.* [14] classifier and anomaly detection methods of [17], [19] in the sense that we segment coronary tree in CTA using hybrid energy formulation. Accordingly, the segment radial information based on the segmented tree is employed in classification to handle both positive and negative remodeling associated with the soft plaques. Experimental results demonstrate that the proposed method achieves a good agreement (detection accuracy of 88.4% with respect to manual annotations), and in-line with anomaly detection methods of [17], [19].
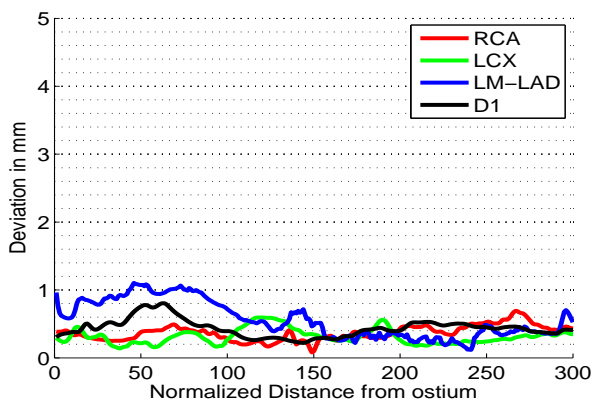
C. CTA Dataset Acquisition

In this study, we have investigated three CTA datasets in context of the soft plaque detection. A first dataset comes from public database of Rotterdam Coronary Artery Evaluation framework. This dataset contains 18 CTA volumes coming from different scanners and different institutes as explained in [26], [27]. The second dataset consisting of 12 clinical CTA volumes was obtained from Guys & St. Thomas's Hospital London. In addition, a third dataset consisting of only two CTA volumes was obtained from Semmelweis University, Budapest Hungary. It should be noted that the multi-vendor data increases the complexity of the plaque detection problem; however, the reproducibility of the method can be validated successfully. Moreover, all the CTA data provides complete ground truth in terms of segment nature (normal or plaque effected), type and position of the plaque in abnormal segments and stenosis information (if any) for the vessel boundary respectively.

II. METHODS

The first step in the plaque detection process is the segmentation of the coronary tree in CTA using a hybrid energy formulation as proposed in Jawaid *et al.* [28]. After tree extraction, we performed the skeletonization using fast marching implementation of the thinning algorithm of Van *et al.* [29]. As the plaque detection method heavily relies upon the centreline accuracy, we evaluated the deviation error with respect to manual reference ground truth as presented in Fig. 1. The visual comparison for complete coronary vasculature is presented in Fig. 1a, whereas the deviation error for individual segments (RCA, LCX, LAD and D1) is shown in Fig. 1b. After generating the tree skeleton, we used 17-segment model of American Heart Association (AHA) [30] to label the individual segment present in respective coronary tree. In the subsequent step, we employed segment-wise centerlines to extract cylindrical volume using interpolation in 3D space. In the final step, the cross-section based cylindrical volume is used in a support vector machine framework to identify abnormalities in segment respectively. For a mathematical interpretation of the paper, let I defines a 3D CTA image and $\mathbf{x}$ represents a spatial
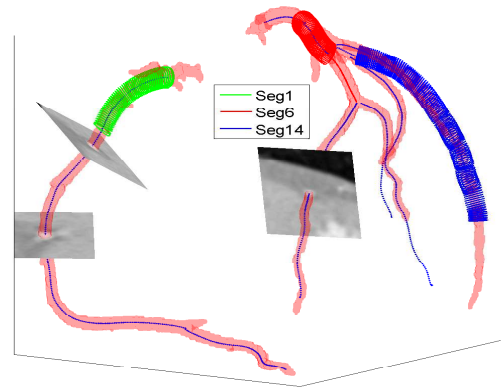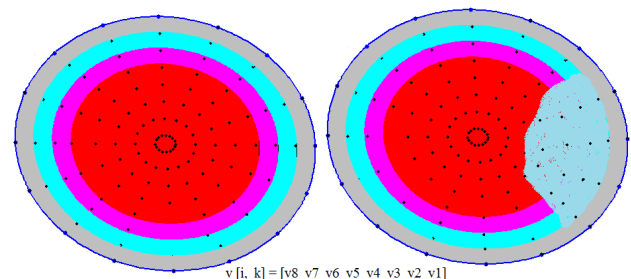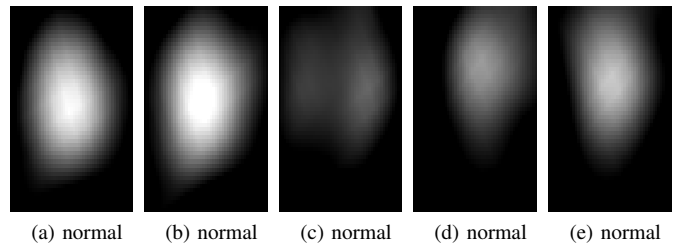
(a) over-riding with reference

Fig. 2. Cylindrical model for coronary segments using 6mm circle. It can be observed that 3D surface is overlaid with centreline (black) along with oblique planes in 3D space. Moreover, blue, red and green contours represent the curved cylindrical approximations for three segments of AHA model.

(b) Deviation error

Fig. 1. Centreline accuracy with respect to reference centreline [27]. (a, c) shows obtained centreline overlain with reference in 3D space, whereas (b, d) represents mean deviation for major segments in millimeters. It can be observed that mean deviation with respect to the reference is less than or around 1mm.

(a) normal   (b) normal   (c) normal   (d) normal   (e) normal

(f) Intensity composition for normal and abnormal coronary cross sections.

Fig. 3. Cross-section based visualization of coronary segment. (a)-(e) represents grey scale visualization for sequential cross sections, whereas (f) shows colour interpretation in context of concentric rings (dots). It can be observed from (f) that left represents a normal cross section with adequate flow of blood, whereas right shows a plaque leading to blood obstruction.

location in domain Ω. Moreover, it is important to mention that the high intensity based calcifications are regularized in a pre-processing stage to optimize the non-calcified detection as reported in [13]–[16], [18], [21], [31], [32]. Accordingly, the high intensity plaques were assigned lumen intensity value to minimize to work with-in the scope of this research.

A. Cylindrical Modelling of Coronary Segments

In order to identify the intensity in-homogeneity along the coronary tree, we employed the ideal of the mean radial profile. However, in contrast to conventional 2D image based profiles, we used an extended version to detect intensity abnormality in 3D vessel structures. Accordingly, we extracted oblique cross sections along the length of segment by substituting $\mathbf{n}_{xyz} = [n_x, n_y, n_z]^T$ (normal of the plane) and $\mathbf{c}_{xyz}$ (centreline point at respective location) in by (1).

$$\mathbf{n}_{xyz} \cdot (\mathbf{x} - \mathbf{c}_{xyz}) = 0 \qquad (1)$$

The normal of the plane is computed using consecutive points of the centreline to precisely follow the vessel orientation.

To effectively represent the coronary segments, we used the diameter for cylindrical model to be 6 mm, as it represents the

maximum possible expansion of the normal coronary structure in CTA [11], [33]. This 6mm modelling is illustrated in Fig. 2 where it can be observed that the circumference of the cylindrical model serves interface between lumen and the background. In the subsequent step, we computed the customized radial profile for the coronary segment using discrete approximations as expressed by (2).

$$v[i, k] = \frac{1}{L} \sum_{t=1}^{L} I(r_i, \theta_t, q_k) \, \forall i, k, \ i = 1, ..., 8, \ \ k = 1, ...K \quad (2)$$

where q_k represents the kth cross sectional of coronary segment and K defines the total number of points along the

length of the segment. L denotes the total number of projected rays, which is set equal to 16 in our model and the respective projection angle is computed as $\theta_t = t\left(\frac{\pi}{8}\right)$. Moreover, i denotes the concentric ring formed at radius $r_i = 0.4(9-i)$mm. It is important to mention that the discretization parameters are selected to achieve a balance between profile accuracy and processing load. Accordingly, this sampling interval used for radial and cylindrical axis represents 0.4mm (isotropic voxel size), 22.5° angular interval projects 16 rays on the sampling plane for estimation of the radial profile on respective plane. Moreover, the formulation for radius r_i parameter reflects that concentric rings are numbered in an inward fashion, i.e. the outer ring is labeled as v_1 with inner most ring named as v_8 as shown in visual illustration of cross sections in Fig. 3f. It can be observed that in general inner rings (v_5 to v_8) define the blood filled lumen and outer rings (v_1 to v_4) define the interface between lumen and the CTA background.

The concentric ring based labeling phenomena is further demonstrated in Fig. 4, where the intensity response is presented along the length of the coronary segment. It can be observed that four external rings defining external interface assumes low intensity values and remain stable irrespective of the normal or abnormal cross-section, whereas the internal four rings reflect the contrast filled blood in terms of high intensity. Moreover, it can be observed from the figure that normal cross-sections lead to stable response for the inner rings, whereas the presence of low intensity material results in significant concavities for inner four rings (see Fig. 4b).
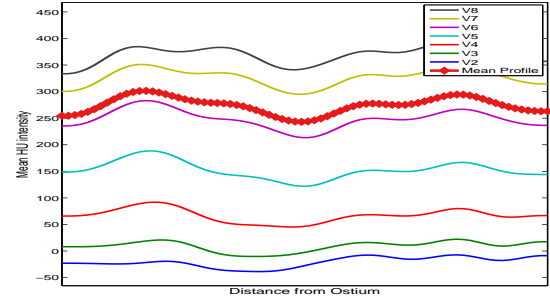
Accordingly, we start with the assumption that this concavity property of the diseases segments can be effectively used in support vector machine based classification. In the subsequent step, we computed mathematical representation (s) of coronary segment using intensity response of four inner rings as follows:

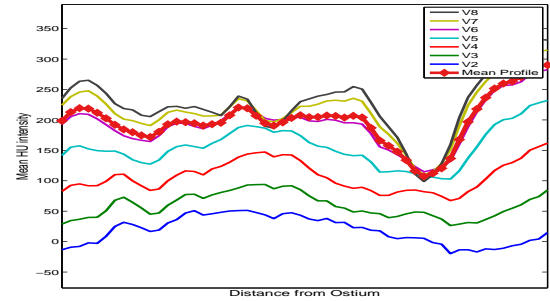$$s[k] = \frac{1}{4}\sum_{i=5}^{8} v[i,k], \ \forall k, \ k = 1...K \qquad (3)$$

The mean segment representation of the coronary segment often undergoes short term transitions, which are smoothed with the help of moving average operation. Accordingly, we compute the smoothed statistical representation of the segment in terms of moving mean and moving standard deviation using a [1] by [3] moving window as expressed in (4). Moreover, it can be visually observed from Fig. 3f that the different coronary segments have variable lengths. Accordingly, this length variation is apportioned in this step with the help of spline-based interpolation to construct fixed length characteristic functions μ'_s, σ'_s (each having 100 samples) for respective coronary segments.

$$\sigma_s[k] = \sqrt{\frac{1}{(2n+1)-1}\sum_{i=-n}^{n}(s[k+i]-\mu[k])^2},$$

$$\mu_s[k] = \frac{1}{2n+1}\sum_{i=-n}^{n}s[k+i], \ \forall k, \ k = 1,...,K \qquad (4)$$

(a) CTA Volume 6 Segment 1 (normal).

(b) CTA Volume 5 Segment 2 (abnormal)

Fig. 4. Intensity plot for 8 concentric rings (v_1 to v_8) for two segments (normal and abnormal). It can be observed that central ring (v_8) exhibits HU intensity and outer ring (v_1) assumes lower intensity value. Moreover, the mean representation of the coronary segment is computed by averaging the four inner rings (v_8) - (v_5).

B. SVM Based Segment Classification

1) Feature Based Representation for Coronary Segments: The computation of fixed length characteristic function is followed with SVM based differentiation of the plaque effected coronary segments. The performance of the SVM classifier heavily relies on the selected features, as distinctive features helps classifier in optimal performance, whereas ambiguous features lead to poor accuracy. In context of the non-calcified plaque detector SVM, the intensity plays most important role as it is the only indicator of the non-calcified plaques. Accordingly, we derived hand-crafted features capable to project intensity variations before application of the SVM classifier. Accordingly, we extracted the features by splitting the segment characteristic functions μ'_s and σ'_s into m windows as expressed in (5).

$$f_\mu[m] = \sum_{n=1}^{5} \mu'_s[n+5(m-1)], \forall m = 1,2,...,20$$

$$f_\sigma[m] = \sum_{n=1}^{5} \sigma'_s[n+5(m-1)], \forall m = 1,2,...,20 \qquad (5)$$

The idea of m windows is used to exploit the relative variations in intensity along the length of the segment. However, selection of appropriate number of windows is a challenging task as it rationalizes the feature vector dimension at the cost of approximation error. Relationship between subsets and the

approximation error is presented in Fig. 5, where it can be observed that the quantization error is inversely proportional to the number of subsets, i.e. approximation improves as the number of windows is increased. In order to maintain a balance between the accuracy and the feature vector size, we defined number of subsets m equal to 20, as the quantization error becomes steady for $m = 20$ as illustrated in the Fig. 5. Accordingly, the discriminative capability of subset based extracted features (f_μ and f_σ) to distinguish the intensity patterns in to two classes is illustrated in Fig. 6 (see Fig. 6a - reffig:fig8f).

Furthermore, an additional parameter namely mid-lumen intensity f_{mid} is added to improve the performance of the SVM classifier. Mathematical formulation for the mid lumen intensity is expressed by (6), i.e. mid-lumen response is acquired by modelling the intensity of the central concentric ring v_8.

$$f_{mid}[m] = \frac{1}{5} \sum_{n=1}^{5} v_8[n + 5(m-1)], \forall m = 1, 2, ..., 20 \quad (6)$$

The visual justification for the additional feature mid lumen intensity is presented in Fig. 6c and 6f. Apparently f_{mid} replicates the distribution pattern of f_μ; however, this feature encodes the concentration of contrast medium in the lumen centre along the length of the segment. It is important to mention that a non-calcified plaque located at the start of the coronary segment results in lower intensity in the mid of lumen; hence, the segment must be labelled as abnormal. However, due to the stable mean and variance along the segment, classifier may erroneously identify segment as normal. Accordingly, the mid lumen feature f_{mid} ensures that the classifier takes into account not only the intensity variations but the mid-lumen response of segment for efficient classification. Next, we concatenate three feature sets f_μ, f_σ and f_{mid} to obtain a feature based representation $\mathbf{Fx}_i$ for respective coronary segment with dimensions [1 x 60].

2) SVM Classification Framework: For a support vector machine based classifier, the input data consists of a feature space along with training labels, i.e. N feature vectors of the form $\mathbf{X}_n$ and the associated binary labels Y_n defining the class of feature vector as normal or diseased as expressed by (7). Here d represent the dimensions of feature vector, i.e. defined equal to 60 in this work and N represents total number of samples in the classifier test.

$$D = \left\{ (\mathbf{X}_n, Y_n) \,|\, \mathbf{X}_n \subseteq R^d, Y_n \subseteq \{-1, 1\} \right\}_{n=1}^{N} \quad (7)$$

In context of the binary classification problem, the support vector machine computes an optimal hyperplane by minimizing the norm of weights for ideal segregation; however, a slack variable is often integrated to relax the constraints for a feasible solution as expressed in (8).

$$min \, |\mathbf{w}|^2 + P \sum_{i=1}^{n} \varepsilon_i \quad (8)$$

$$subject\ to: Y_n \left(\mathbf{w}^T \mathbf{X_n} + b \right) \geq 1 - \varepsilon_i,\ \varepsilon_i \geq 0, for\ i = 1, 2, ...n$$

where $P = 10^0$ defines the penalty cost, i.e. it is responsible for regularizing the influence of individual support vectors

in the classification. A small value of P leads to quick and inaccurate classification, i.e. having frequent violations, whereas high value results in slow and accurate classification using hard margin in classification. For mapping data into higher space, we employed a non-linear radial basis Gaussian kernel with σ set equal to 1.

III. RESULTS

A. Results for SVM Classification

The first step towards verification of the results is the formulation of ground truth reference. For this research work, the ground truth comes along with the CTA image data, i.e. all CTA images accompany manual expert-based segment-wise labels. The corresponding labels indicate the status of the coronary segment in terms normal or plaque affected, and for plaque affected segments the ground truth further reveals the potential position. As the scope of this work is detection of plaque in coronary vasculature using SVM classifier, we therefore employed ground truth in context of normal versus plaque affected coronary segments.

Accordingly, we evaluated the plaque detection performance of the SVM classifier by extracting a total of 344 (200 normal, 144 abnormal) segments from 32 CTA volumes. The statistical validation for detection performance has been performed using Leave One Out (LOO) cross validation as shown in Fig. 7. It is important to mention that for N samples, LOO validation method employs $N-1$ samples in the training and One sample in testing. From computational point of view, LOO validation consumes extra time in comparison with $K - fold$ validation; however, it reveals the true efficiency of the SVM model, as every sample is evaluated individually. It can be observed that a promising sensitivity rate of 92% is achieved. Moreover, positive predictive value for SVM classifier is 81.4%, negative predictive value is 86.9% and overall accuracy of soft plaque detection is equal to 84.6%. A relatively high value for these metrics reveal that the automated detection methods is capable of detecting non-calcified plaques with a good agreement with human expert, which is ultimate theme of any computer assisted application.

Next, we evaluated the performance of the SVM model on three data sets individually to validate the generalization of our model. In this evaluation, we extracted test segments individually from three datasets (66 from Rotterdam, 76 from St. Thomas and 36 from Semmelweis) and SVM classification results are presented in Fig. 8. In the subsequent step, we used the trained SVM classifier to investigate the impact of feature vector dimensions on the classifier efficiency. In this test we used 122 coronary segments extracted from 3 datasets (70 normal and 52 abnormal according to the manual ground truth) and compared the classifier performance in terms of accuracy and processing time. It has been observed that the windowed mean and deviation based 40 features lead to a classification accuracy of 76.8%, where the addition of mid-lumen f_{mid} and features improved the classifier accuracy by approximately 8%. Moreover, the comparative analysis demonstrates that the further increase in the feature space dimensions show only a marginal improvement in the classifier accuracy, while the computational time increases significantly. These results lead to the conclusion that the classifier performance becomes

(a) 2 subsets (b) 4 subsets (c) 5 subsets (d) 10 subsets (e) 20 subsets (f) 25 subsets

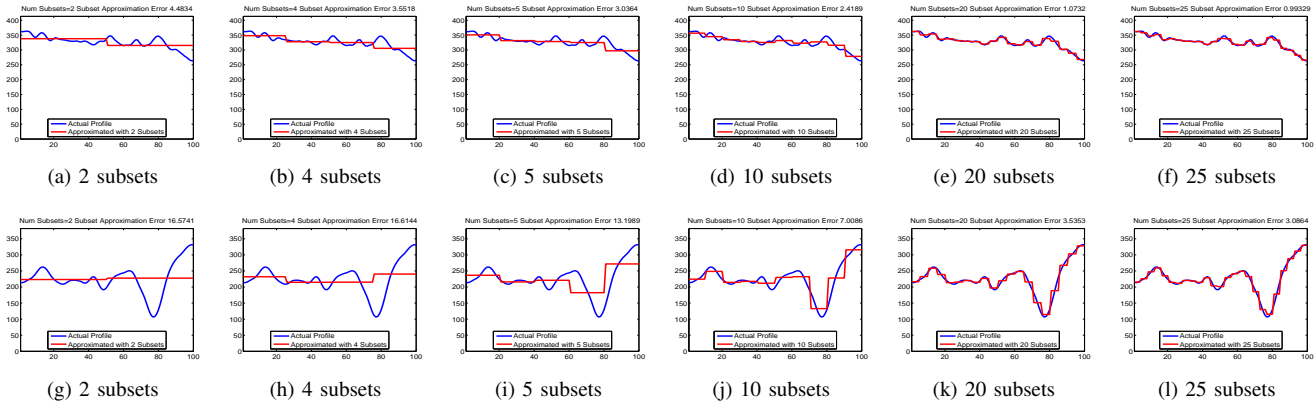(g) 2 subsets (h) 4 subsets (i) 5 subsets (j) 10 subsets (k) 20 subsets (l) 25 subsets

Fig. 5. Subset based signal representation to reduce the dimensions of the feature vector. It can be observed from a pairwise comparison that both normal (top) and abnormal (below) segments can be adequately represented using 20-25 subsets. The top row represents normal segment and bottom row represents abnormal segments.

(a) Normal windowed mean. (b) Normal windowed std. (c) Normal mid-voxel intensity.

(d) Abnormal windowed mean. (e) Abnormal windowed std. (f) Abnormal mid-voxel intensity.
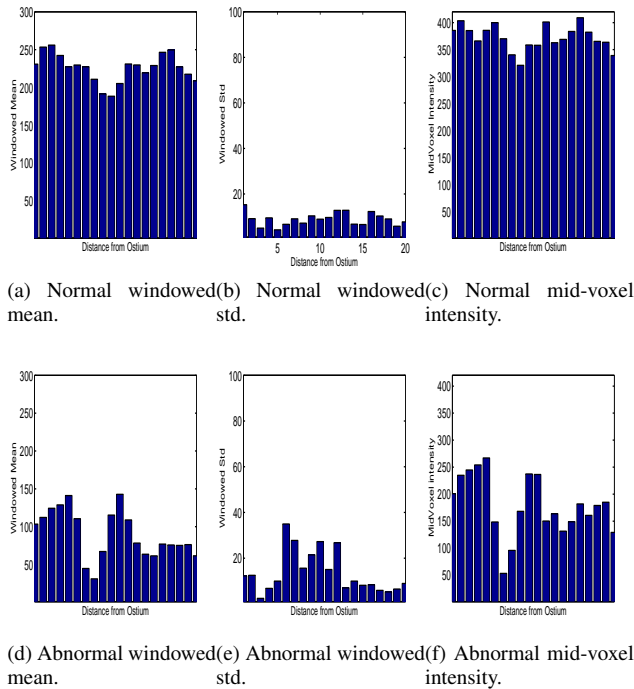
Fig. 6. illustration for the segment descriptor features. (a, c) shows stable values for moving mean and deviation for a normal segment, whereas (b, d) shows unexpected jumps for a soft plaque effected segment. Moreover (e, f) reflects the discriminatory power of mid lumen intensity i.e normal segment (e) assumes higher HU in contrast to abnormal segment (f) effected with low density soft plaque.

resistant to the feature vector dimensions at a certain point due to the redundancy of features.

IV. DISCUSSION

It can be observed from the performance graph (Fig. 7) that the overall performance for proposed SVM detection model is 84.6% with respect to the clinician based manual detected ground truth, with a sensitivity of 92% and specificity of 80.3%. Moreover, it can be observed from Fig. 8 that plaque detection performance remain consistent around 82% for three
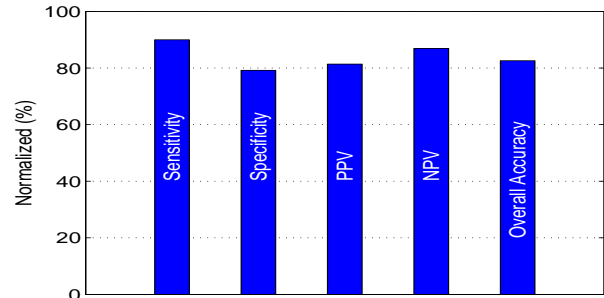

Fig. 7. Plaque detection performance of the SVM classifier. Leave one OUT based cross correlation shows an overall detection accuracy around 84.6%, with reasonable sensitivity, specificity, PPV and NPV rates.
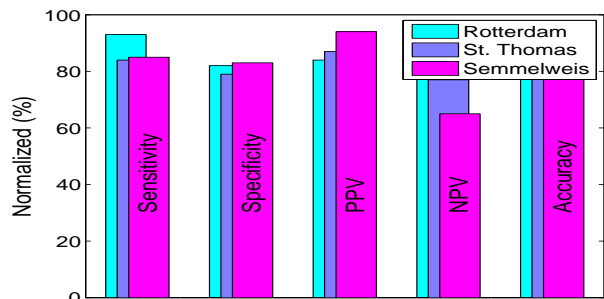

Fig. 8. SVM classifier performance for three individual datasets. The overall accuracy is centred at 80% with a consistent sensitivity and specificity ratio for three datasets.

individual datasets. The detection performance for three individual datasets can be further explained based on the fact that a "significant dip" in the segment profile ensures greater accuracy for the classifier. Accordingly, a large number of severe plaque instances in the Rotterdam data results in higher sensitivity, whereas the relative low accuracy for Semmelweis CTA data indicates the absence of severe plaque instances. In addition to the manual ground truth based validation, the efficiency of the proposed model is compared with state-of-

the-art plaque detection methods of Wei *et al.* [14] (sensitivity of 93%), Lankton *et al.* [16] (sensitivity of 88%) and Tessmann *et al.* [17] (sensitivity of 79%) to establish a correlation with the reported literature. The future work aims to extend this work for a quantitative analysis of plaque in abnormal marked coronary segments. One possible extension is the use of deep learning framework to avoid the computation of hand crafted features for SVM model. Accordingly, we believe that the automated detection of non-calcified plaque can significantly increase the diagnostic of clinical experts to reduce cardiac fatalities.

V. Conclusion

We proposed an efficient method for automated detection of non-calcified plaques in cardiac CTA imagery. The innovation of this work is statistical representation of coronary segments, and the support vector machine based 2-class interpretation of respective segments. Accordingly, the proposed model delivers a very good detection rate for non-calcified plaques with respect to manual expert detections. In context of the future expansion of this work, there exists many potential extensions. An important aspect is to use the detected plaques for precise voxel-wise quantification of total plaque volume, which is the most important indicator of coronary heart disease. Another possible extension is to employ the deep learning in plaque detection process. This can allow auto feature extraction and minimize the user burden by eliminating the need of hand crafted features. In addition, one potential extension is to obtain the ground truth from multiple human experts and evaluate the plaque performance of the proposed method with respect of independent observers in context of inter-observer agreement.

Acknowledgment

References

[1] S. Waxman, F. Ishibashi, and J. E. Muller, "Global, regional, and national age-sex specific all-cause and cause-specific mortality for 240 causes of death, 1990-2013: a systematic analysis for the global burden of disease study 2013," *Lancet*, vol. 385, no. 9963, pp. 117–171, 2015.

[2] U. K. NHS. Coronary Heart Disease, statistics for united kingdom. Available at http://www.nhs.uk/Conditions/Coronary-heart-disease/Pages/Introduction.aspx(2016/11/11).

[3] W. H. Organization. Cardiovascular diseases CVDs, the global statistics. Available at http://www.who.int/mediacentre/factsheets/fs317/en/(2016/11/11).

[4] T. Flohr and B. Ohnesorge, "Multi-slice ct technology," in *Multi-slice and Dual-source CT in Cardiac Imaging*. Springer, 2007, pp. 41–69.

[5] M. S. David C. Levin and D. Fischman. Coronary CTA, a cost-effective alternative to cardiac catheterization for the evaluation of cad, study suggests. Available at https://www.sciencedaily.com/releases/2010/04/100421162617.htm (2016/12/07).

[6] S. C. Saur, H. Alkadhi, L. Desbiolles, G. Székely, and P. C. Cattin, "Automatic detection of calcified coronary plaques in computed tomography data sets," in *International Conference on Medical Image Computing and Computer-Assisted Intervention*. Springer, 2008, pp. 170–177.

[7] G. Brunner, U. Kurkure, D. R. Chittajallu, R. P. Yalamanchili, and I. A. Kakadiaris, "Toward unsupervised classification of calcified arterial lesions," in *International Conference on Medical Image Computing and Computer-Assisted Intervention*. Springer, 2008, pp. 144–152.

[8] I. Išgum, A. Rutten, M. Prokop, and B. van Ginneken, "Detection of coronary calcifications from computed tomography scans for automated risk assessment of coronary artery disease," *Medical physics*, vol. 34, no. 4, pp. 1450–1461, 2007.

[9] B. Mohr, S. Masood, and C. Plakas, "Accurate lumen segmentation and stenosis detection and quantification in coronary cta," in *Proceedings of 3D Cardiovascular Imaging: a MICCAI segmentation challenge workshop*, 2012.

[10] R. Virmani, A. P. Burke, A. Farb, and F. D. Kolodgie, "Pathology of the vulnerable plaque," *Journal of the American College of Cardiology*, vol. 47, no. 8s1, pp. C13–C18, 2006.

[11] R. Shahzad, H. Kirisli, C. Metz, H. Tang, M. Schaap, L. van Vliet, W. Niessen, and T. van Walsum, "Automatic segmentation, detection and quantification of coronary artery stenoses on cta," *The International Journal of Cardiovascular Imaging*, vol. 29, no. 8, pp. 1847–1859, 2013.

[12] S. Waxman, F. Ishibashi, and J. E. Muller, "Detection and treatment of vulnerable plaques and vulnerable patients novel approaches to prevention of coronary events," *Circulation*, vol. 114, no. 22, pp. 2390–2411, 2006.

[13] M. E. Clouse, A. Sabir, C.-S. Yam, N. Yoshimura, S. Lin, F. Welty, P. Martinez-Clark, and V. Raptopoulos, "Measuring noncalcified coronary atherosclerotic plaque using voxel analysis with mdct angiography: a pilot clinical study," *American Journal of Roentgenology*, vol. 190, no. 6, pp. 1553–1560, 2008.

[14] J. Wei, C. Zhou, H.-P. Chan, A. Chughtai, P. Agarwal, J. Kuriakose, L. Hadjiiski, S. Patel, and E. Kazerooni, "Computerized detection of noncalcified plaques in coronary ct angiography: Evaluation of topological soft gradient prescreening method and luminal analysis," *Medical Physics*, vol. 41, no. 8, p. 081901, 2014.

[15] F. Renard and Y. Yang, "Image analysis for detection of coronary artery soft plaques in mdct images," in *5th IEEE International Symposium on Biomedical Imaging: From Nano to Macro*. IEEE, 2008, pp. 25–28.

[16] S. Lankton, A. Stillman, P. Raggi, and A. Tannenbaum, "Soft plaque detection and automatic vessel segmentation," in *12th International Conference on Medical Image Computing and Computer Assisted Intervention (MICCAI)*. Springer Berlin Heidelberg, 2009, pp. 25–33.

[17] M. Tessmann, F. Vega-Higuera, D. Fritz, M. Scheuering, and G. Greiner, "Multi-scale feature extraction for learning-based classification of coronary artery stenosis," in *SPIE Medical Imaging*. International Society for Optics and Photonics, 2009, pp. 726 002–726 002.

[18] H. Brodoefel, C. Burgstahler, A. Sabir, C.-S. Yam, F. Khosa, C. D. Claussen, and M. E. Clouse, "Coronary plaque quantification by voxel analysis: dual-source mdct angiography versus intravascular sonography," *AJR. American Journal of Roentgenology*, vol. 192, no. 3, p. W84, 2009.

[19] M. A. Zuluaga, I. E. Magnin, M. H. Hoyos, E. J. D. Leyton, F. Lozano, and M. Orkisz, "Automatic detection of abnormal vascular cross-sections based on density level detection and support vector machines," *International Journal of Computer Assisted Radiology and Surgery*, vol. 6, no. 2, pp. 163–174, 2011.

[20] I. Steinwart, D. R. Hush, and C. Scovel, "Density level detection is classification." in *NIPS*, 2004, pp. 1337–1344.

[21] Y. Li, W. Chen, K. Liu, Y. Wu, Y. Chen, C. Chu, B. Fang, L. Tan, and S. Zhang, "A voxel-map quantitative analysis approach for atherosclerotic noncalcified plaques of the coronary artery tree," *Computational and Mathematical Methods in Medicine*, vol. 2013, 2013.

[22] S. Achenbach, F. Moselewski, D. Ropers, M. Ferencik, U. Hoffmann, B. MacNeill, K. Pohle, U. Baum, K. Anders, I.-k. Jang *et al.*, "Detection of calcified and noncalcified coronary atherosclerotic plaque by contrast-enhanced, submillimeter multidetector spiral computed tomography," *Circulation*, vol. 109, no. 1, pp. 14–17, 2004.

[23] A. W. Leber, A. Becker, A. Knez, F. von Ziegler, M. Sirol, K. Nikolaou, B. Ohnesorge, Z. A. Fayad, C. R. Becker, M. Reiser *et al.*, "Accuracy of 64-slice computed tomography to classify and quantify plaque volumes

in the proximal coronary system," *Journal of the American College of Cardiology*, vol. 47, no. 3, pp. 672–677, 2006.

[24] T. Schepis, M. Marwan, T. Pflederer, M. Seltmann, D. Ropers, W. G. Daniel, and S. Achenbach, "Quantification of non-calcified coronary atherosclerotic plaques with dual-source computed tomography: comparison with intravascular ultrasound," *Heart*, vol. 96, no. 8, pp. 610–615, 2010.

[25] M. Otsuka, N. Bruining, N. C. Van Pelt, N. R. Mollet, J. M. Ligthart, E. Vourvouri, R. Hamers, P. De Jaegere, W. Wijns, R. T. Van Domburg *et al.*, "Quantification of coronary plaque by 64-slice computed tomography: a comparison with quantitative intracoronary ultrasound," *Investigative radiology*, vol. 43, no. 5, pp. 314–321, 2008.

[26] W. Theo. The Great Challenge, coronary artery stenoses detection and quantification evaluation framework. Available at http://coronary.bigr.nl/stenoses/(2016/11/11).

[27] H. Kirişli, M. Schaap, C. Metz, A. Dharampal, W. B. Meijboom, S. Papadopoulou, A. Dedic, K. Nieman, M. De Graaf, M. Meijs *et al.*, "Standardized evaluation framework for evaluating coronary artery stenosis detection, stenosis quantification and lumen segmentation algorithms in computed tomography angiography," *Medical image analysis*, vol. 17, no. 8, pp. 859–876, 2013.

[28] M. M. Jawaid, R. Rajani, P. Liatsis, C. C. Reyes-Aldasoro, and G. Slabaugh, "A hybrid energy model for region based curve evolution-application to cta coronary segmentation," *Computer Methods and Programs in Biomedicine*, vol. 144C, pp. 189–202, 2017.

[29] R. Van Uitert and I. Bitter, "Subvoxel precise skeletons of volumetric data based on fast marching methods," *Medical Physics*, vol. 34, no. 2, pp. 627–638, 2007.

[30] G. L. Raff, A. Abidov, S. Achenbach, D. S. Berman, L. M. Boxt, M. J. Budoff, V. Cheng, T. DeFrance, J. C. Hellinger, R. P. Karlsberg *et al.*, "Scct guidelines for the interpretation and reporting of coronary computed tomographic angiography," *Journal of Cardiovascular Computed Tomography*, vol. 3, no. 2, pp. 122–136, 2009.

[31] F. Renard and Y. Yang, "Image segmentation for detection of soft plaques in multidetector ct images," in *2008 IEEE Southwest Symposium on Image Analysis and Interpretation*, March 2008, pp. 121–124.

[32] A. Ponnapan. Automatic Soft Plaque Detection from CTA, georgia institute of technology. Available at https://pdfs.semanticscholar.org/5ad6/81ce27f6720ee2c9c00298226dcef3

d01e7b.pdf(2016/11/11).

[33] J. Dodge, B. G. Brown, E. L. Bolson, and H. T. Dodge, "Lumen diameter of normal human coronary arteries. influence of age, sex, anatomic variation, and left ventricular hypertrophy or dilation." *Circulation*, vol. 86, no. 1, pp. 232–246, 1992.